

# Electrical and stability performance of anode-supported solid oxide fuel cells with strontium- and magnesium-doped lanthanum gallate thin electrolyte

Weimin Guo, Jiang Liu\*, Yaohui Zhang

*College of Chemistry, South China University of Technology, Guangzhou 510640, Guangdong, PR China*

Received 14 September 2007; received in revised form 9 January 2008; accepted 13 January 2008

Available online 25 January 2008

## Abstract

Anode-supported solid oxide fuel cells (SOFCs) comprising NiO–samarium-doped ceria (SDC) ( $\text{Sm}_{0.2}\text{Ce}_{0.8}\text{O}_{1.9}$ ) composite anode, thin tri-layer electrolyte, and  $\text{La}_{0.6}\text{Sr}_{0.4}\text{Co}_{0.8}\text{Fe}_{0.2}\text{O}_3$  (LSCF)– $\text{La}_{0.9}\text{Sr}_{0.1}\text{Ga}_{0.8}\text{Mg}_{0.2}\text{O}_{3-\delta}$  (LSGM) composite cathode were fabricated. The thin tri-layer consisting of an 11- $\mu\text{m}$  thick LSGM electrolyte layer and a 12- $\mu\text{m}$  thick  $\text{La}_{0.4}\text{Ce}_{0.6}\text{O}_{1.8}$  (LDC) layer on each side of the LSGM was prepared by centrifugal casting and co-firing technique. The performance of the cells operated with humidified  $\text{H}_2$  as fuel and ambient air as oxidant showed a maximum power density of  $1.23 \text{ W cm}^{-2}$  at  $800^\circ\text{C}$ . A stability test of about 100 h was carried out and some deterioration of output power was observed, while the open circuit voltage (OCV) kept unchanged. Impedance measurements showed that both the electrolyte ohmic resistance and the electrode polarization increased with time and the latter dominated the degradation.

© 2008 Elsevier Ltd. All rights reserved.

**Keywords:** SOFCs;  $\text{La}_{0.9}\text{Sr}_{0.1}\text{Ga}_{0.8}\text{Mg}_{0.2}\text{O}_{3-\delta}$ ; Centrifugal casting; Co-firing; Stability

## 1. Introduction

Solid oxide fuel cells (SOFCs) operating in the intermediate temperature range ( $500\text{--}800^\circ\text{C}$ ) (IT-SOFCs) have received great attention because a relative large material selection range and a reasonable performance can be realized at the same time [1,2]. Doped zirconia, doped ceria, and doped  $\text{LaGaO}_3$  have been selected as the electrolytes for SOFCs. Ytria-stabilized zirconia (YSZ) is the most commonly used electrolyte for SOFCs due to its pure oxygen-ion conduction and its stability both in oxidizing and reducing atmospheres. However, the ionic conductivity of this conventional electrolyte below  $1000^\circ\text{C}$  is not satisfying. Despite excellent performance of anode-supported YSZ electrolyte SOFCs operated around  $800^\circ\text{C}$ , searching for alternative electrolyte with higher conductivity has been attracting much interest. Doped ceria such as gadolinium-doped ceria (GDC) or samarium-doped ceria (SDC) has much higher ionic conductivity than YSZ at lower temperatures but the major drawback is its mixed electronic/ionic conduction properties under the fuel reducing atmosphere [3]. Compared to YSZ and

doped ceria, perovskite-type strontium and magnesium-doped lanthanum gallate (LSGM) is a new kind of electrolyte material and has not been thoroughly investigated. While some stability problems may occur in some cases for LSGM, it might become an alternative electrolyte that can allow operating temperature below  $800^\circ\text{C}$ , due to its high oxygen ionic conductivity ( $0.15 \text{ S cm}^{-1}$  at  $800^\circ\text{C}$ ), high oxygen transport number, good chemical stability over a wide oxygen partial pressure range ( $10^{-22}$  to 1 atm), and good mechanical strength [4].

Some electrolyte-supported or thick film LSGM SOFCs have been fabricated and shown good performance at  $800^\circ\text{C}$  [5–8]. However, the ohmic resistance mainly from the electrolyte in these cells still dominates the cell performance in the reduced temperature range. Recently, many efforts have been contributed to fabricate SOFC single cells with anode-supported thin LSGM electrolyte [9,10]. A deep understanding of the effect of the extensive chemical reactions between LSGM and electrodes or ionic migration during high-temperature co-firing on the performance of the SOFCs has been conveyed [10,11]. La diffusion at the anode/electrolyte interface and inter-diffusion of Ga and Co across the cathode may result in a serious problem with a thinner electrolyte. The Co diffusion into the LSGM creates a conducting phase that penetrates from the cathode toward the anode to reduce the real LSGM thickness. It has been suggested

\* Corresponding author. Tel.: +86 20 2223 6168; fax: +86 20 2223 6168.  
E-mail address: [jiangliu@scut.edu.cn](mailto:jiangliu@scut.edu.cn) (J. Liu).

that  $\text{La}_{0.4}\text{Ce}_{0.6}\text{O}_{1.8}$  (LDC) buffer layer must be introduced to minimize reactions and inter-diffusion between LSGM and the Ni-based anode or the Co-contained cathode [5]. Despite the promising results obtained from the anode-supported single SOFC with thin LSGM film, there is a lack of demonstration of long-term stability under high power output, even though there are some reports about stability test of SOFCs with thick LSGM electrolyte [5,7].

In the present work, a centrifugal casting technique was applied to fabricate thin LDC/LSGM/LDC tri-layer on NiO–SDC ( $\text{Sm}_{0.2}\text{Ce}_{0.8}\text{O}_{1.9}$ ) anode substrates. SOFCs with dense thin LDC/LSGM/LDC layers were prepared by co-firing, with no evidence of deleterious reactions. SOFC testing exhibited relative high power densities. A cell maintaining at a constant current of  $1 \text{ A cm}^{-2}$  was tested for 95 h at  $800^\circ\text{C}$ . The measured voltage at this current dropped from 0.699 V at the beginning to about 0.607 V after the test and the maximum power density decreased from  $1.08 \text{ W cm}^{-2}$  to  $0.81 \text{ W cm}^{-2}$ . The experimental results were carefully discussed.

## 2. Experimental

### 2.1. Powder preparation

$\text{La}_{0.9}\text{Sr}_{0.1}\text{Ga}_{0.8}\text{Mg}_{0.2}\text{O}_{3-\delta}$  (LSGM) powder was synthesized by solid-state reaction. Stoichiometric amount of  $\text{La}_2\text{O}_3$ ,  $\text{SrCO}_3$ ,  $\text{Ga}_2\text{O}_3$ , and  $\text{MgO}$  were mixed in ethanol and ball-milled for 20 h. The mixture was dried and pre-fired at  $1000^\circ\text{C}$  for 4 h, then pressed into pellets, finally sintered at  $1250^\circ\text{C}$  for 21 h.  $\text{La}_{0.4}\text{Ce}_{0.6}\text{O}_{1.8}$  (LDC) powder was also synthesized by solid-state reaction of  $\text{La}_2\text{O}_3$  and  $\text{CeO}_2$  after firing at  $1250^\circ\text{C}$  for 21 h. The  $\text{Sm}_{0.2}\text{Ce}_{0.8}\text{O}_{1.9}$  (SDC) powder was prepared using a citric-nitrate process and calcined at  $800^\circ\text{C}$  for 2 h [12]. Nickel oxide (NiO) powder was obtained by the precipitation method, using  $\text{Ni}(\text{NO}_3)_2 \cdot 6\text{H}_2\text{O}$  as the raw material and ammonia as the precipitant. The precipitate was calcined at  $400^\circ\text{C}$  for 2 h.  $\text{La}_{0.6}\text{Sr}_{0.4}\text{Co}_{0.8}\text{Fe}_{0.2}\text{O}_3$  (LSCF) powder was produced by a combined citrate–EDTA complexing method and the primary powder was calcined at  $950^\circ\text{C}$  for 5 h [13].

All the powders were characterized with an X-ray diffractometer (XD-3A, Shimadzu, Japan) with  $\text{Cu K}\alpha$  radiation. The selected  $2\theta$  range was from  $20^\circ$  to  $80^\circ$  scanning at a step of  $0.02^\circ$ . The XRD patterns were analyzed and determined with MDI Jade 5.1 and PCPDFWIN 1.10 software.

### 2.2. Cell fabrication

The as-prepared NiO and SDC powders were mixed in a weight ratio of 6:4. After the mixture with 15 wt% starch as pore former was mixed and ground in an agate mortar for 2 h, the anode powders were pressed into pellets of 13 mm in diameter and 0.6 mm in thickness under a pressure of 300 MPa. The green pellets were pre-sintered at  $1000^\circ\text{C}$  for 4 h to obtain the NiO–SDC anode substrates. Tri-layer electrolytes LDC/LSGM/LDC were sequentially deposited on NiO–SDC anode substrates by centrifugal casting technique [14]. The technique is simple, fast, and economical. The coating thickness can

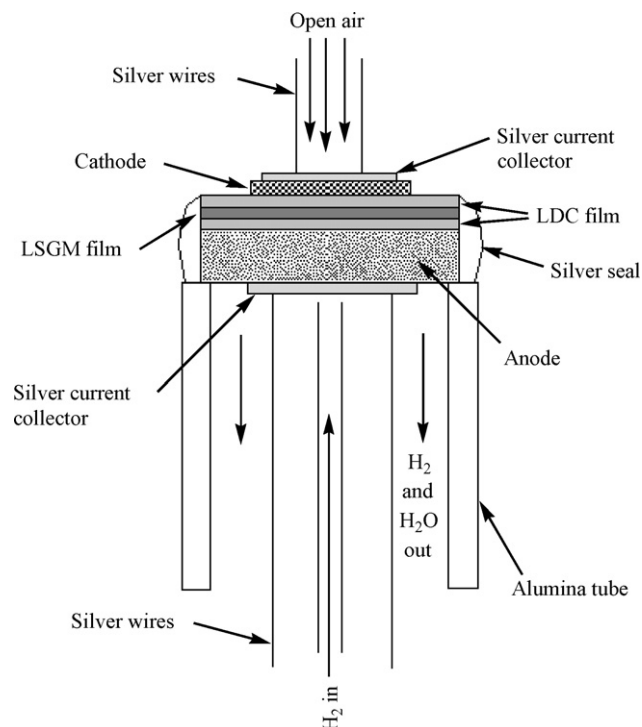


Fig. 1. Schematic illustration of the single-cell testing set.

be easily and accurately controlled over a large range. LDC and LSGM slurry suspensions were prepared by mixing 0.5 g of each powder and an organic vehicle of ethylcellulose (6 wt%) and terpineol (94 wt%) in a weight ratio of 1:1 with 100 mL ethanol, and sonicating for 1 h. The NiO–SDC substrates were placed in vessels with flat bottom, and a proper amount of slurry was added into each vessel along with some more ethanol. The vessels were then placed in a centrifuge with a radius of about 20 cm, and the centrifuge was operated for 30 min at 4000 rpm. In the centrifugal field, the ceramic particles in the slurry were forced down to the surface of the substrate to form a coating. After the centrifuge process, the supernatant was decanted and the film prepared was dried in ambient air for half an hour. Then, the next layer was deposited. In this way, layers of LDC, LSGM, and LDC were centrifugal deposited sequentially on the anode supports. The thickness of the LSGM and LDC layers was controlled by the amount of slurry. The deposited pellets were dried in open air, and then sintered at  $1400^\circ\text{C}$  for 4 h. The porous cathode was prepared using a mixture of LSCF and LSGM in a weight ratio of 1:1 with an ethylcellulose–terpineol vehicle. The mixture was applied on the electrolyte, followed by a pure LSCF layer, and fired at  $1100^\circ\text{C}$  for 1 h in air.

### 2.3. Cell testing

A single cell was assembled by attaching a cell pellet to one end of an alumina tube using silver paste (DAD-87, Shanghai Research Institute of Synthetic Resin, Shanghai, China) as sealant and joint material (Fig. 1). The cells were tested with an electrochemical instrument (Autolab PGSTAT30, Eco Chemie, Holland). Hydrogen passing over the anode was controlled at

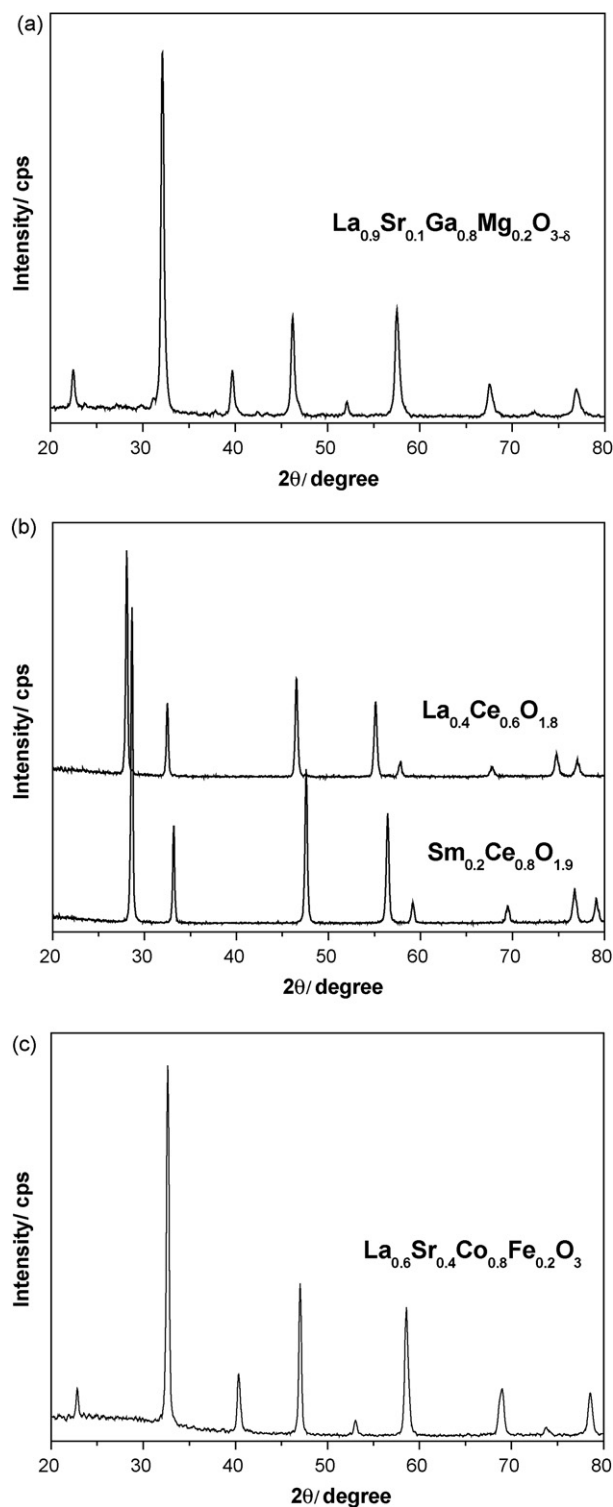


Fig. 2. XRD patterns of (a) LSGM powders prepared by solid-state reaction, (b) LDC powders prepared by solid-state reaction and SDC powders prepared by citrate-nitrate process, and (c) LSCF powders prepared by combined citrate-EDTA complexing method.

a flow rate of  $75 \text{ mL min}^{-1}$ , while the cathode was exposed to ambient air. After the NiO-contained anode was reduced at  $600^\circ\text{C}$  in  $\text{H}_2$  for several hours, the performance of the cell was tested from  $600^\circ\text{C}$  to  $800^\circ\text{C}$  with an interval of  $50^\circ\text{C}$ .

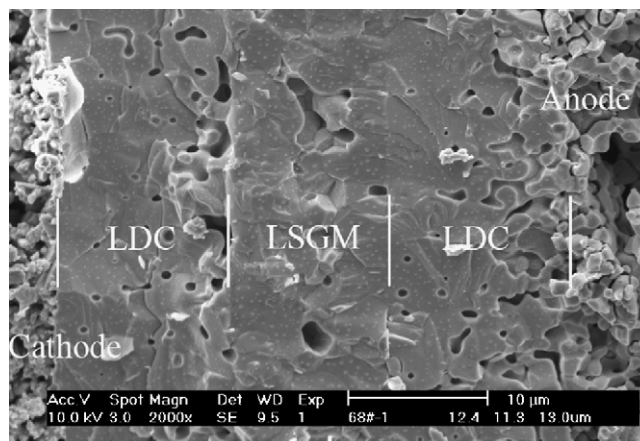


Fig. 3. Cross-sectional SEM image of a typical LDC/LSGM/LDC tri-layer electrolyte with portions of the Ni-SDC anode support and LSGM-LSCF cathode.

Impedance spectra were measured typically in the frequency range from 0.1 Hz to 100 kHz under open-circuit conditions. The tested cell was fractured and examined by a scanning electron microscope (Philips XL-30FEG, Holland).

### 3. Results and discussion

#### 3.1. Characterization of powders

The XRD analysis shows that the XRD pattern of the as prepared LSGM powder (Fig. 2a) matches well with the diffraction data for a perovskite phase. The patterns for LDC and SDC show the standard cubic fluorite structure and a full single phase (Fig. 2b). The XRD pattern of LSCF powder (Fig. 2c) shows good agreement with expected peaks for a perovskite phase, with no indication of second phases.

#### 3.2. Microstructure of cell

Fig. 3 shows a cross-sectional SEM image of the LDC/LSGM/LDC tri-layer along with the surrounding anode

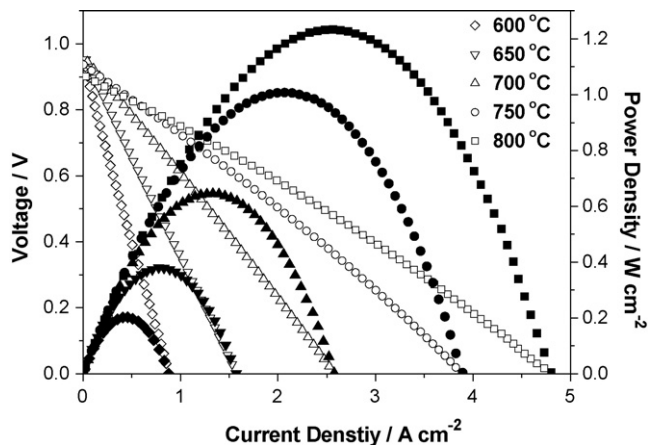


Fig. 4. Voltage and power densities vs. current density of a thin LDC/LSGM/LDC tri-layer electrolyte SOFC operated on air and humidified hydrogen.

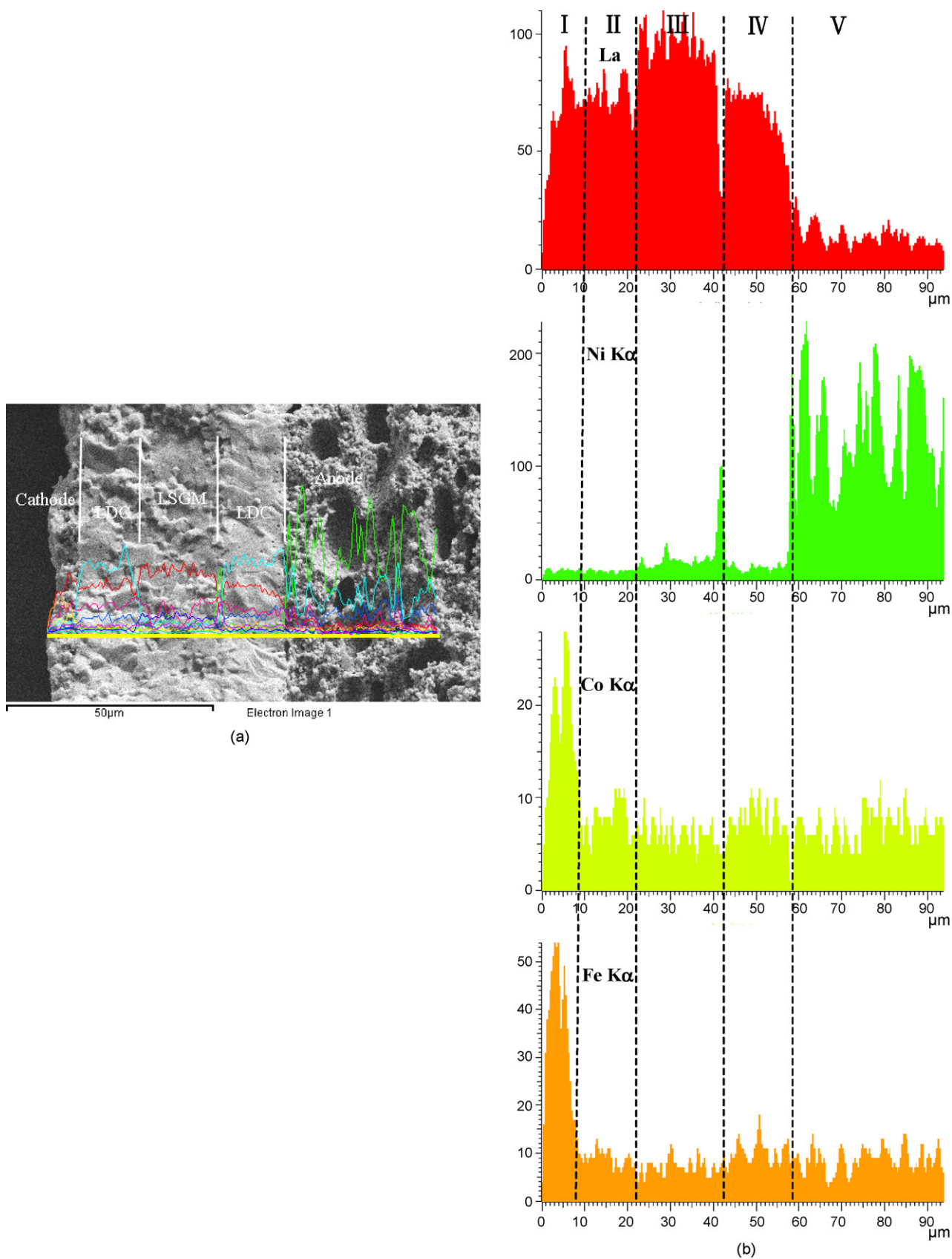


Fig. 5. EDX linear scan analysis results on the cross-section of the LDC/LSGM/LDC tri-layer electrolyte, Ni-SDC anode support and LSGM-LSCF cathode after long-term testing (a) SEM image; (b) EDX shows the La, Ni, Co and Fe element distribution over a 94 μm range: (I) LSCF-LSGM cathode, (II) LDC buffer layer, (III) LSGM electrolyte, (IV) LDC buffer layer, and (V) Ni-SDC anode.

and cathode of a single cell. No peel-off and crack were found at the interface between the LSGM and LDC layers. The LSGM and LDC layers were relatively dense with some closed pores. There was good intimate contact between the LSGM and LDC layers and the surrounding electrodes, showing that the materials sintered well together, although their sintering properties are somewhat distinctly different. The LSGM layer and LDC layers on either side are about 11  $\mu\text{m}$  and 12  $\mu\text{m}$  thick, respectively.

### 3.3. Cell output performance

Fig. 4 shows the  $I$ - $V$  curves and the corresponding power densities for the single cell with LDC/LSGM/LDC tri-layer electrolyte. The values of the OCV are quite similar to those reported by Lin et al. with a 9  $\mu\text{m}$  LSGM and 7–10  $\mu\text{m}$  LDC tri-layer electrolyte cell [15]. The OCVs are all lower than that of a thick LSGM single cell ( $\sim 1.1$  V) tested in similar conditions. Lin et al. suggested that the lower OCV is not caused by gas leakage across the electrolyte based on the facts of dense electrolyte, low measured gas leakage rate, and stable OCV value with changing gas flow rate. To identify whether metal cations had migrated across the electrode/electrolyte interfaces, the cell was characterized by EDX after power measurement. Fig. 5 shows the results of EDX linear scans for elements distribution (La, Ni, Co, and Fe) across the cross-sectional area. It was observed that the LDC buffer layer between cathode and electrolyte successfully blocked the diffusion of Fe and Co cations from the cathode into the LSGM film, probably ascribed the results to the relatively low firing temperature for cathode. However, obvious Ni peaks were seen in the interface of LSGM and LDC film closed to anode side and also appeared in LSGM film, presumably due to migration during the high temperature co-firing. Introduction of Ni into LSGM will induce electronic p-type conduction in the electrolyte resulting in lower OCV [16,17]. Another similar work with thicker LSGM layer (50  $\mu\text{m}$ ) and LDC layers (25  $\mu\text{m}$ ) reported by Bi et al. [10,11] showed higher OCV of 1.043 V at 800  $^{\circ}\text{C}$ , but the power density was lower, 0.86  $\text{W cm}^{-2}$  compared with 1.12  $\text{W cm}^{-2}$  at 750  $^{\circ}\text{C}$  reported by Lin et al. and 1.23  $\text{W cm}^{-2}$  at 800  $^{\circ}\text{C}$  of the present work, presumably due to higher resistance caused by the thicker electrolyte layers which also producing higher OCV through blocking metal migration more effectively. Some optimization on the thickness of the elec-

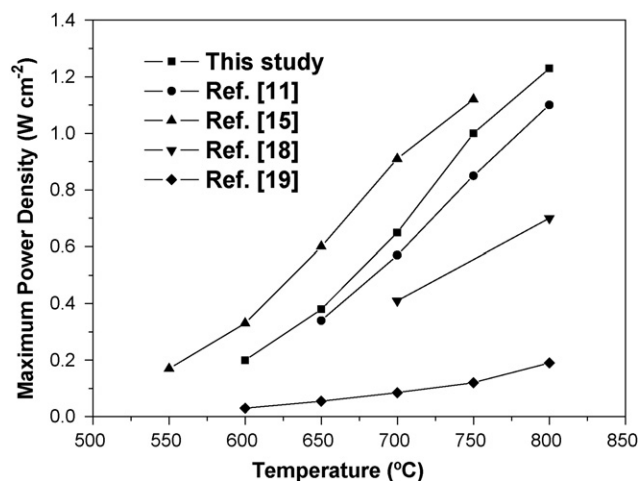


Fig. 6. Maximum power densities vs. temperature for the present SOFC compared with prior reports from Refs. [11,15,18,19].

trolyte layers should be made to get the best performance of such cells.

The maximum power densities shown in Fig. 4 are 1.23, 1.0, 0.65, 0.38 and 0.20  $\text{W cm}^{-2}$  at 800, 750, 700, 650, and 600  $^{\circ}\text{C}$ , respectively. Fig. 6 compares the maximum power densities for the present LDC/LSGM/LDC tri-layer electrolyte SOFC with some prior reported data for LSGM electrolyte cells fabricated by co-firing [11,15,18,19]. The compositions of these cells are listed in Table 1. Despite the difference of materials used for anodes and cathodes, the power densities of these cells with and without buffer layers show general dependence on the thickness of the electrolyte, i.e., a cell with thinner electrolyte gives higher power density.

### 3.4. Impedance spectroscopy

Fig. 7 shows the impedance spectra of a typical single cell measured under open-circuit at temperatures from 600  $^{\circ}\text{C}$  to 800  $^{\circ}\text{C}$  using a four-probe configuration. The intercept with the real-axis at the highest frequency represents the ohmic resistance of the electrolyte (ohmic resistance from other sources can be neglected). The measured specific ohmic resistance across the LDC/LSGM/LDC tri-layer electrolyte film is 0.086  $\Omega \text{ cm}^2$  at 800  $^{\circ}\text{C}$ , lower than the calculated value 0.13  $\Omega \text{ cm}^2$  based on

Table 1  
Compositions of LSGM electrolyte SOFCs fabricated by co-firing

Cell sources	Anode	Anode buffer layer	Electrolyte	Cathode buffer layer	Cathode
Present work	Ni-Sm <sub>0.2</sub> Ce <sub>0.8</sub> O <sub>1.9</sub> (60:40 wt%)	La <sub>0.4</sub> Ce <sub>0.6</sub> O <sub>1.8</sub> (LDC) (12 $\mu\text{m}$ )	LSGM (11 $\mu\text{m}$ )	LDC (12 $\mu\text{m}$ )	La <sub>0.6</sub> Sr <sub>0.4</sub> Co <sub>0.8</sub> Fe <sub>0.2</sub> O <sub>3</sub> -LSGM (50:50 wt%)
Ref. [11]	Ni-Gd <sub>0.1</sub> Ce <sub>0.9</sub> O <sub>1.95</sub> (60:40 wt%)	La <sub>0.45</sub> Ce <sub>0.55</sub> O <sub>2-8/2</sub> (LDC) (25 $\mu\text{m}$ )	LSGM (50 $\mu\text{m}$ )	LDC (25 $\mu\text{m}$ )	La <sub>0.9</sub> Sr <sub>0.1</sub> CoO <sub>3</sub> -LDC (60:40 wt%)
Ref. [15]	Ni-La <sub>0.4</sub> Ce <sub>0.6</sub> O <sub>1.8</sub> (LDC) (60:40 wt%)	LDC (8 $\mu\text{m}$ )	LSGM (9 $\mu\text{m}$ )	LDC (8 $\mu\text{m}$ )	La <sub>0.6</sub> Sr <sub>0.4</sub> Co <sub>0.8</sub> Fe <sub>0.2</sub> O <sub>3</sub> -LSGM (50:50 wt%)
Ref. [18]	Ni-Sm <sub>0.2</sub> Ce <sub>0.8</sub> O <sub>1.9</sub> (52:48 mol%)	-	LSGM (130 $\mu\text{m}$ )	-	La <sub>0.6</sub> Sr <sub>0.4</sub> CoO <sub>3</sub>
Ref. [19]	Ni-La <sub>0.4</sub> Ce <sub>0.6</sub> O <sub>1.8</sub> (LDC) (50:50 wt%)	LDC (15 $\mu\text{m}$ )	LSGM (1 mm)	-	La <sub>0.6</sub> Sr <sub>0.4</sub> Co <sub>0.8</sub> Fe <sub>0.2</sub> O <sub>3</sub> -LSGM (50:50 wt%)

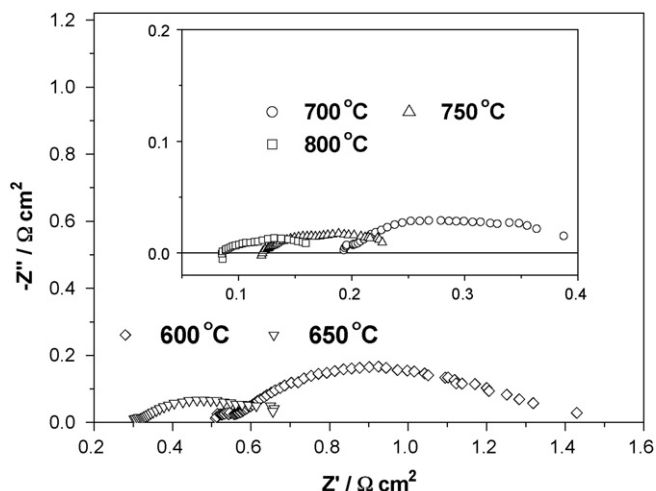


Fig. 7. Electrochemical impedance spectra of a single SOFC measured under open-circuit conditions in air and humidified hydrogen.

prior reported bulk LSGM conductivity of  $0.12 \text{ S cm}^{-1}$  and LDC of  $0.02 \text{ S cm}^{-1}$  at  $800^\circ\text{C}$  [20,21]. This is most likely because the bulk conductivity of LDC in a single cell under operating condition is higher than that measured directly on the electrolyte under air atmosphere [11]. The relative lower resistance of LDC/LSGM/LDC tri-layer electrolyte film and the high output performance of the single cell indicate that the reactions inducing high resistance products between LSGM and NiO or cathode were effectively prevented by the LDC buffer layers. In the impedance spectra, the lowest frequency real axis intercept provides a measure of the total cell resistance, the width of the impedance arcs on the real-axis is the polarization resistance, which includes reaction and transport resistances from both the anode and cathode.

The polarization resistance, ohmic resistance and total resistance as determined from the impedance spectra are shown in Fig. 8. At temperatures below  $700^\circ\text{C}$ , the polarization resistance is higher than the ohmic resistance. While there may be some opportunities to improve the cell performance by optimizing the

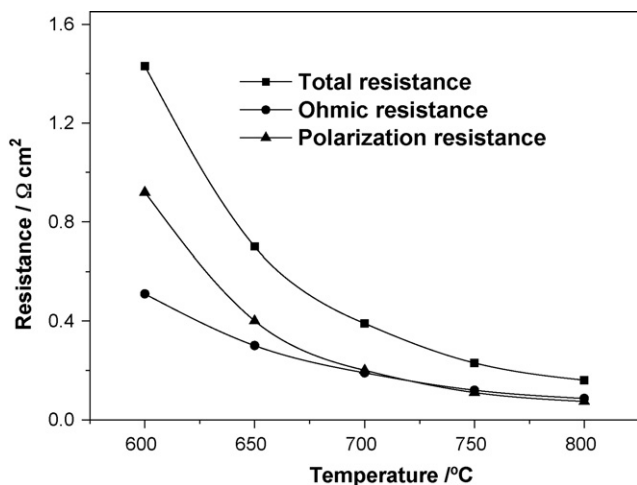


Fig. 8. Tri-layer electrolytes resistance, electrode polarization resistance, and total cell resistance as determined by impedance spectra.

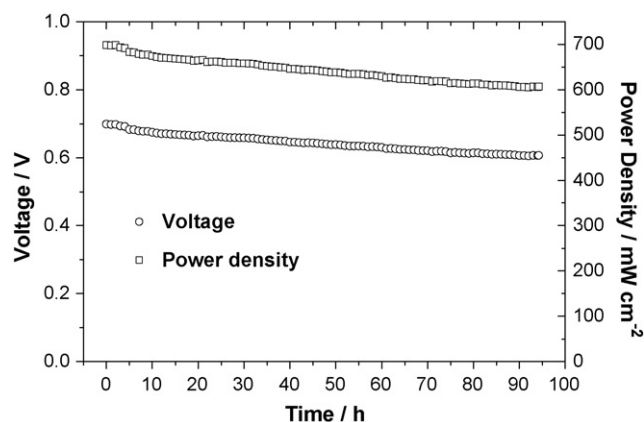


Fig. 9. Voltage and power density vs. time for a single Ni-SDC/LDC/LSGM/LDC/LSCF-LSGM cell operated at a constant current of  $1 \text{ A cm}^{-2}$ .

thickness of the layers composing the tri-layer electrolyte, there is potential to get a better performance at reduced temperatures by improving the electrodes.

### 3.5. Cell stability

A stability test of the cell was carried out under a constant current density of  $1000 \text{ mA cm}^{-2}$  with a  $30 \text{ mL min}^{-1}$   $\text{H}_2$  flow rate at  $800^\circ\text{C}$ . The cell voltage at this current was recorded as a function of time. The cell was tested for about 100 h and the results are shown in Fig. 9. Note the cell used for this test had been tested 10 days before to get performance data and then it was cooled down and placed in open air. At the beginning of the stability test, the cell performance was slightly lower than that of the first time test. Then it gradually degraded with time at a rate of about  $1 \text{ mV h}^{-1}$ . A comparison of output performance measured before and after the stability test is presented in Fig. 10. The maximum power density drops from  $1.08 \text{ W cm}^{-2}$  before the test to  $0.81 \text{ W cm}^{-2}$  after 95 h. It is obvious that the OCV does not change with time. This fact suggests that there is little transition metal diffusing from the electrodes to the electrolyte during cell operation. In other words, the deterioration of the cell is not caused by higher electronic conduction of the electrolyte

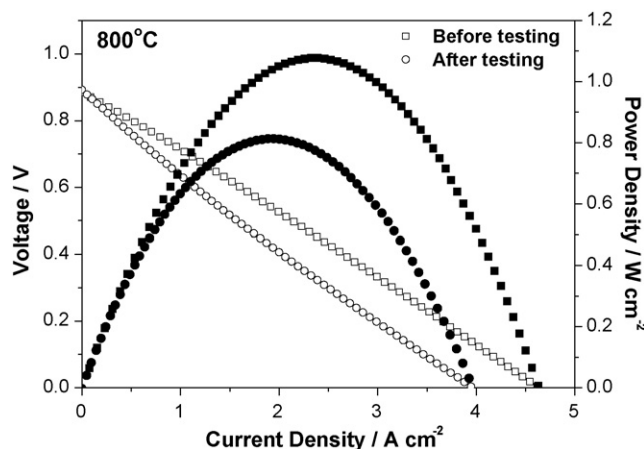


Fig. 10. Comparison of cell performance measured before and after a stability test of 95 h.

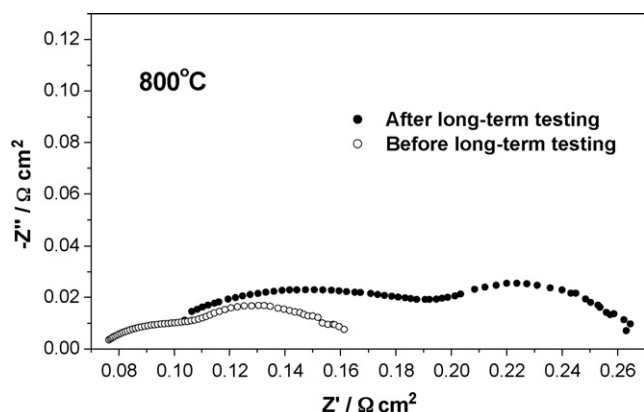


Fig. 11. Comparison of the electrochemical impedance spectra measured before and after stability testing.

induced by transition metal diffusion to the LSGM layer. The electrochemical impedance spectra in Fig. 11 show that both the electrode polarization and ohmic electrolyte resistance after 95 h stability test are higher than that before the test. While the increase of ohmic resistance is about  $0.03 \Omega \text{ cm}^2$ , the increase of the electrode polarization is  $0.1 \Omega \text{ cm}^2$ , three times of the electrolyte.

Considering the unchanging OCV with time and the significant increase of electrode polarization, we presume that the

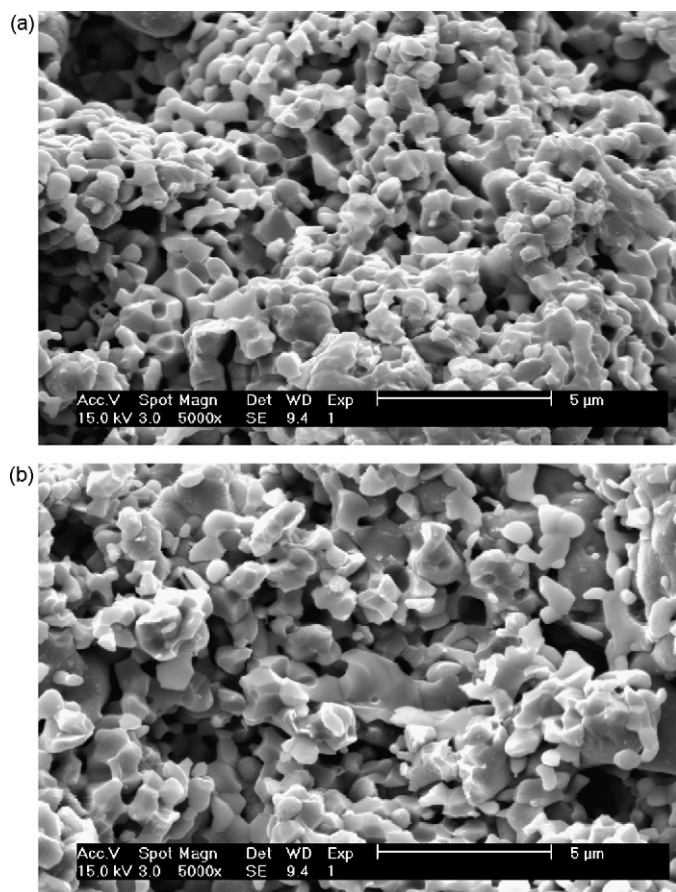


Fig. 12. SEM images of a NiO–SDC anode with humidified  $\text{H}_2$  as fuel operated for (a) several hours and (b) 95 h.

deterioration of the cell performance over time is mainly caused by degradation of electrodes or electrode–electrolyte interfaces. The influence of nickel metal coarsening in the porous Ni–SDC anode has been indicated by some prior researchers [22], and is assured further by the SEM images in Fig. 12, showing particles in the anode becomes coarser with operating time. Some further studies are in progress and the details will be reported in the future.

#### 4. Conclusions

Anode-supported SOFCs with dense thin LDC/LSGM/LDC tri-layer electrolyte, Ni–SDC cermet anode, and LSCF–LSGM composite cathode were successfully fabricated using centrifugal casting and co-sintering technique. The maximum power densities were 1.23, 1.0, 0.65, 0.38 and  $0.20 \text{ W cm}^{-2}$  at 800, 750, 700, 650 and  $600^\circ\text{C}$ , respectively. The good performance and low ohmic resistance showed that there was no significant formation of deleterious interfacial phases. A  $12\text{-}\mu\text{m}$  thick of LDC buffer layer cannot completely avoid the diffusion of Ni from anode to LSGM electrolyte during high temperature co-firing resulting in a lower OCV. A 95-h stability of the cells was monitored at  $800^\circ\text{C}$  under a constant current density of  $1000 \text{ mA cm}^{-2}$ . While the OCV of the cell did not change with time, some deterioration of the cell output was observed. Based on the difference of the impedance spectra and the SEM images of the anode obtained before and after the stability test, we presume that the deterioration of the cell performance over time is mainly caused by degradation of the electrodes or electrode–electrolyte interfaces. Further investigation is needed to determine the detail mechanisms of the degradation.

#### Acknowledgements

The authors gratefully acknowledge the financial support from 863 Program of National High Technology Research Development Project of China (Grant No. 2007AA05Z136), the Department of Science and Technology of Guangdong Province (2005B50101007) and the Department of Education of Guangdong Province (B15N9060210).

#### References

- [1] N.Q. Minh, *J. Am. Ceram. Soc.* 76 (1993) 563.
- [2] S.C. Singhal, *Solid State Ionics* 135 (2000) 305.
- [3] M. Mogensen, N.M. Sammes, G.A. Tompsett, *Solid State Ionics* 129 (2000) 63.
- [4] T. Ishihara, H. Matsuda, Y. Takita, *J. Am. Chem. Soc.* 116 (1994) 3801.
- [5] K.Q. Huang, J.-H. Wan, J.B. Goodenough, *J. Electrochem. Soc.* 148 (2001) A788.
- [6] Z.H. Bi, B.L. Yi, Z.W. Wang, Y.L. Dong, H.J. Wu, Y.C. She, M.J. Cheng, *Electrochem. Solid-State Lett.* 7 (2004) A105.
- [7] J.-H. Wan, J.-Q. Yan, J.B. Goodenough, *J. Electrochem. Soc.* 152 (2005) A1511.
- [8] Z.H. Bi, M.J. Cheng, Y.L. Dong, H.J. Wu, Y.C. She, B.L. Yi, *Solid State Ionics* 176 (2005) 655.
- [9] J.W. Yan, H. Matsumoto, M. Enoki, T. Ishihara, *Electrochem. Solid-State Lett.* 8 (2005) A389.

- [10] J.W. Yan, Z.G. Lu, Y. Jiang, Y.L. Dong, C.Y. Yu, W.Z. Li, J. Electrochem. Soc. 149 (2002) A1132.
- [11] Z.H. Bi, Y.L. Dong, M.J. Cheng, B.L. Yi, J. Power Sources 161 (2006) 34.
- [12] D.H.A. Blank, H. Kruidhof, J. Flokstra, J. Phys. D: Appl. Phys. 21 (1988) 226.
- [13] Z.P. Shao, W.S. Yang, Y. Cong, H. Dong, J.H. Tong, G.X. Xiong, J. Membr. Sci. 172 (2000) 177.
- [14] J. Liu, S.A. Barnett, J. Am. Ceram. Soc. 85 (2002) 3096.
- [15] Y.B. Lin, S.A. Barnett, Electrochem. Solid-State Lett. 9 (2006) A285.
- [16] T. Ishihara, T. Shibayama, M. Honda, H. Nishiguchi, Y. Takita, Chem. Commun. (1999) 1227.
- [17] T. Ishihara, T. Shibayama, H. Nishiguchi, Y. Takita, J. Mater. Sci. 36 (2001) 1125.
- [18] T. Fukui, S. Ohara, K. Murata, H. Yoshida, K. Miura, T. Inagaki, J. Power Sources 106 (2002) 142.
- [19] W.Q. Gong, S. Gopalan, U.B. Pal, J. Power Sources 160 (2006) 305.
- [20] J. Drennan, V. Zelizko, D. Hay, F.T. Ciacchi, S. Rajendran, S.P.S. Badwal, J. Mater. Chem. 7 (1997) 79.
- [21] D. Singman, J. Electrochem. Soc. 113 (1966) 502.
- [22] D. Simwonis, F. Tietz, D. Stover, Solid State Ionics 132 (2000) 241.